Aligned fractures modeled as boundary conditions within saturated porous media and induced anisotropy. A finite element approach.

Juan E. Santos[1], Robiel Martínez Corredor[2] and José M. Carcione[3]

[1] CONICET, Instituto del Gas y del Petróleo, Facultad de Ingeniería, Universidad de Buenos Aires and Department of Mathematics, Purdue University
[2] Facultad de Ingeniería Universidad Nacional de La Plata, Argentina
[3]Istituto Nazionale di Oceanografia e di Geofisica Sperimentale (OGS), Italy

Summary

Fractures in a fluid-saturated poroelastic -Biot- medium are very thin, compliant and highly permeable layers. Fracture apertures in reservoir rocks are on the order of millimeters, much smaller that the wavelengths of the predominant travelling waves. Thus, any finite element (FE) procedure would require extremely fine meshes to represent fractures. Here fractures within a Biot medium are modeled using boundary conditions. Besides, a Biot medium with a dense set of aligned fractures behaves as an effective transversely isotropic and viscoelastic (TIV) medium at the macroscale when the predominant wavelengths are much larger than the average distance between fractures. In this work a set of time-harmonic FE experiments are used to determine the stiffness coefficients of a TIV medium equivalent to a horizontally fractured Biot medium. The methodology is first validated against a theory valid for flow perpendicular to the fracture layering and then applied in the case of patchy gas-brine saturation for which no analytical solutions are available.

Stress-strain relations

$$\tau_{st}(\mathbf{u}) = 2G\varepsilon_{st}(\mathbf{u}_s) + \delta_{st}\left(\lambda_U \nabla\cdot\mathbf{u}_s + \alpha M \nabla\cdot\mathbf{u}_f\right)$$
$$p_f(\mathbf{u}) = -\alpha M \nabla\cdot\mathbf{u}_s - M\nabla\cdot\mathbf{u}_f$$

$\mathbf{u}_s$, $\tilde{\mathbf{u}}_f$: solid and fluid displacements. $\mathbf{u}_f = \phi(\tilde{\mathbf{u}}_f - \mathbf{u}_s)$, $\mathbf{u} = (\mathbf{u}_s, \mathbf{u}_f)$ and ϕ: porosity.

The boundary conditions at a fracture

$\Omega = (0, L_1)\times(0, L_3)$: a Biot medium, Γ: boundary of Ω. Assume that Ω has a set of horizontal fractures $\Gamma^{(f,l)}$, $l = 1, \cdots, J^{(f)}$ each one of length L_1 and aperture h. This set of fractures divides Ω in nonoverlapping rectangles, so that $\Omega = \cup_{l=1}^{J^{(f)}+1} R^{(l)}$. Consider two rectangles $R^{(l)}$ and $R^{(l+1)}$ having as a common side $\Gamma^{(f,l)}$.

$\boldsymbol{\nu}_{l,l}$, $\boldsymbol{\chi}_{l,l+1}$: the unit outer normal and a unit tangent on $\Gamma^{(f,l)}$ from $R^{(l)}$ to $R^{(l+1)}$.

$[\mathbf{u}_\theta] = \left({\mathbf{u}_\theta}^{(l+1)} - {\mathbf{u}_\theta}^{(l)}\right)|_{\Gamma^{(f,l)}}$, $\theta = s, f$: jump of the solid and fluid displacement vectors at $\Gamma^{(f,l)}$. ${\mathbf{u}_s}^{(l)}$: displacement values in $R^{(l)}$.

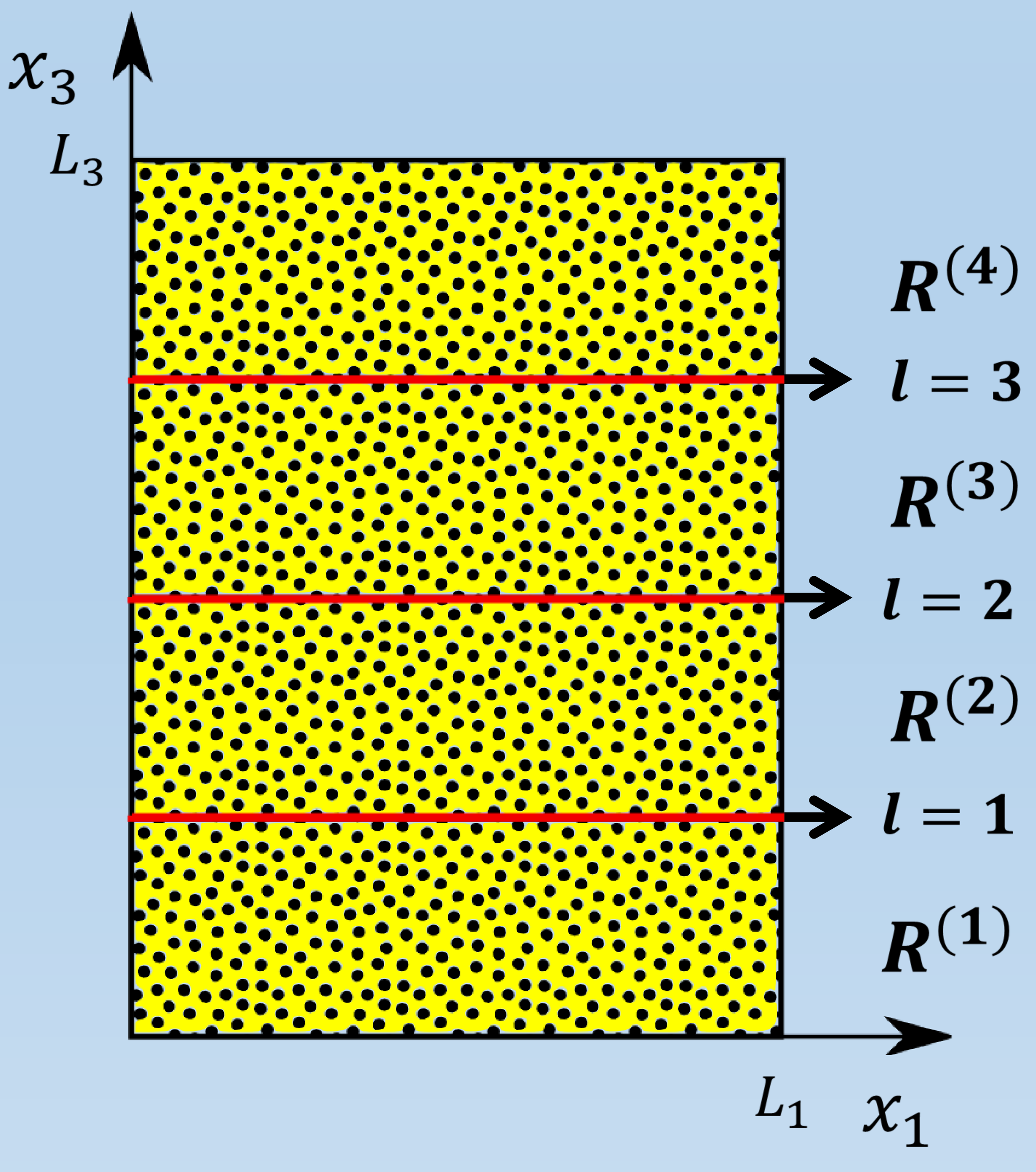

The following boundary conditions on $\Gamma^{(f,l)}$ are derived in Nakagawa, S. and Schoenberg, M. A. (JASA, 2007):

- $[\mathbf{u}_s \cdot \boldsymbol{\nu}_{l,l+1}] =$
  $\eta_N \left(\left(1 - \alpha\tilde{B}(1-\Pi)\right) \boldsymbol{\tau}(\mathbf{u})\nu_{l,l+1} \cdot \boldsymbol{\nu}_{l,l+1} - \alpha \frac{1}{2}\left(\left(-p_f{}^{(l+1)}\right) + \left(-p_f{}^{(l)}\right)\right)\Pi \right)$
- $[\mathbf{u}_s \cdot \boldsymbol{\chi}_{l,l+1}] = \eta_T \boldsymbol{\tau}(\mathbf{u})\nu_{l,l+1} \cdot \boldsymbol{\chi}_{l,l+1}$
- $[\mathbf{u}_f \cdot \boldsymbol{\nu}_{l,l+1}] = \alpha\eta_N \left(-\boldsymbol{\tau}(\mathbf{u})\nu_{l,l+1} \cdot \boldsymbol{\nu}_{l,l+1} + \frac{1}{\tilde{B}}\frac{1}{2}\left(\left(-p_f{}^{(l+1)}\right) + \left(-p_f{}^{(l)}\right)\right)\right)\Pi$
- $\left(-p_f{}^{(l+1)}\right) - \left(-p_f{}^{(l)}\right) = \frac{i\omega\mu\Pi}{\hat{\kappa}}\frac{1}{2}\left(\mathbf{u}_f{}^{(l+1)} + \mathbf{u}_f{}^{(l)}\right) \cdot \boldsymbol{\nu}_{l,l+1}$
- $\boldsymbol{\tau}(\mathbf{u})\nu_{l,l+1} \cdot \boldsymbol{\nu}_{l,l+1} = \boldsymbol{\tau}(\mathbf{u})\nu_{l+1,l} \cdot \boldsymbol{\nu}_{l+1,l}$
- $\boldsymbol{\tau}(\mathbf{u})\nu_{l,l+1} \cdot \boldsymbol{\chi}_{l,l+1} = \boldsymbol{\tau}(\mathbf{u})\nu_{l+1,l} \cdot \boldsymbol{\chi}_{l+1,l}$

η_N, η_T: normal and tangencial fracture compliances,
G, $H_m = K_m + (4/3)G$: dry shear and plane wave modulus, respectively. They are defined in terms of the fracture aperture h as $\eta_N = \frac{h}{H_m}$, $\eta_T = \frac{h}{G}$, $\Pi(\varepsilon) = \tanh\varepsilon/\varepsilon$, $\tilde{B} = \frac{(\alpha M)}{H_U}$, $\varepsilon = \frac{(1+i)}{2}\left(\frac{\omega\mu\alpha\eta_N}{2\tilde{B}\hat{\kappa}}\right)^{1/2}$, $\alpha = 1 - \frac{K_m}{K_s}$.

$\tilde{\mathbf{u}}_s$: solid displacement at the macroscale,
$\sigma_{ij}(\tilde{\mathbf{u}}_s)$, $\varepsilon_{ij}(\tilde{\mathbf{u}}_s)$: stress and strain tensor components of the equivalent TIV medium.

The stress-strain relations for the TIV medium:

- $\sigma_{11}(\tilde{\mathbf{u}}_s) = p_{11}\varepsilon_{11}(\tilde{\mathbf{u}}_s) + p_{12}\varepsilon_{22}(\tilde{\mathbf{u}}_s) + p_{13}\varepsilon_{33}(\tilde{\mathbf{u}}_s)$
- $\sigma_{22}(\tilde{\mathbf{u}}_s) = p_{12}\varepsilon_{11}(\tilde{\mathbf{u}}_s) + p_{11}\varepsilon_{22}(\tilde{\mathbf{u}}_s) + p_{13}\varepsilon_{33}(\tilde{\mathbf{u}}_s)$
- $\sigma_{33}(\tilde{\mathbf{u}}_s) = p_{13}\varepsilon_{11}(\tilde{\mathbf{u}}_s) + p_{13}\varepsilon_{22}(\tilde{\mathbf{u}}_s) + p_{33}\varepsilon_{33}(\tilde{\mathbf{u}}_s)$
- $\sigma_{23}(\tilde{\mathbf{u}}_s) = 2p_{55}\varepsilon_{23}(\tilde{\mathbf{u}}_s)$
- $\sigma_{13}(\tilde{\mathbf{u}}_s) = 2p_{55}\varepsilon_{13}(\tilde{\mathbf{u}}_s)$
- $\sigma_{12}(\tilde{\mathbf{u}}_s) = 2p_{66}\varepsilon_{12}(\tilde{\mathbf{u}}_s)$

To determine the above coefficients, we applied five compressibility and shear FE numerical tests to a representative 2D sample of the fractured poroelastic material.

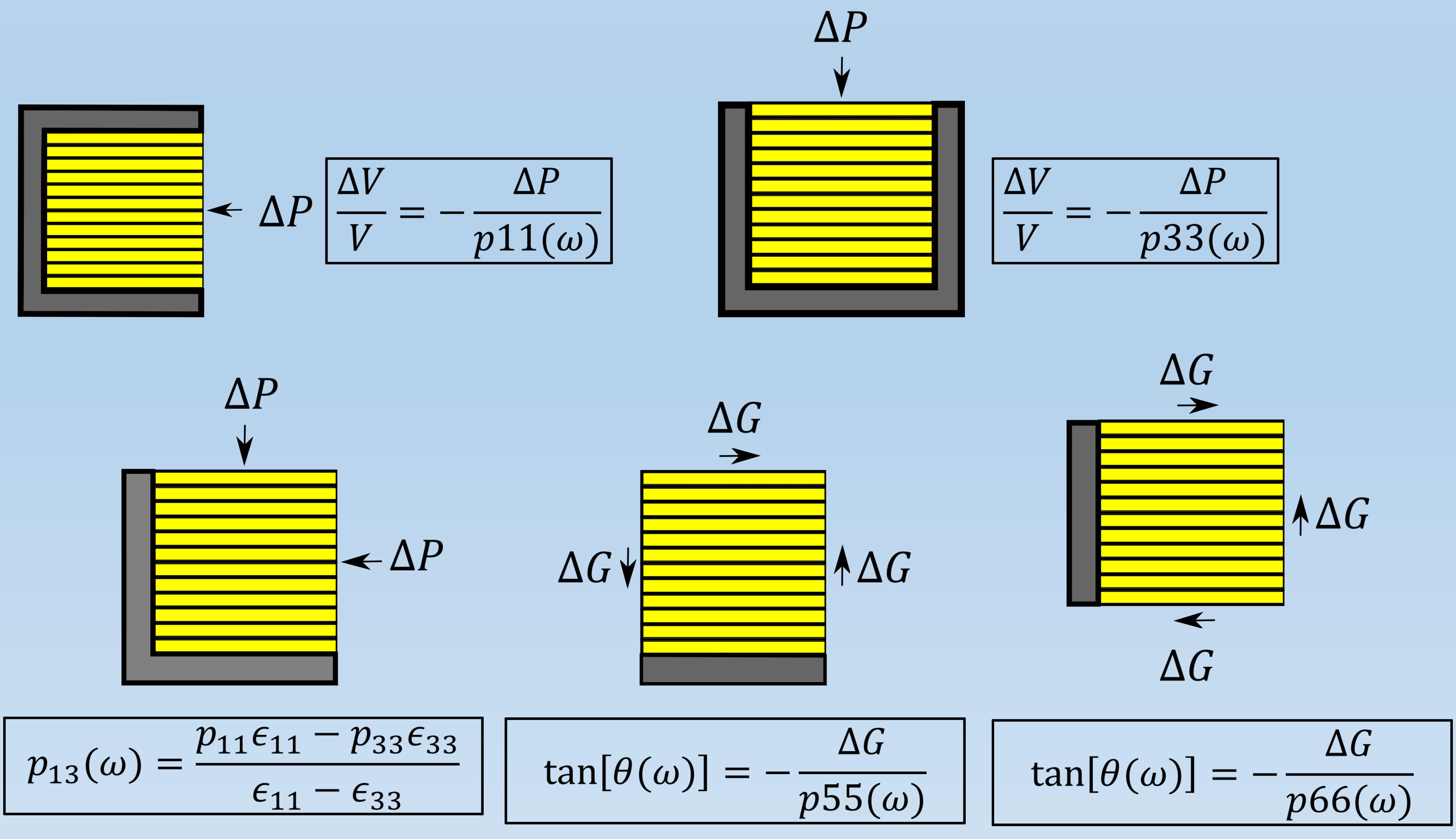

Numerical examples

In all the experiments we used square samples of side length 4 m, with 19 fractures at equal distance of 20 cm and fracture aperture 1 mm. Both background and fractures have grain density ρ_s=2700 kg/m^3 and bulk modulus K_s=36 GPa.

- The first experiment (Figures 1 and 2) validate the FE procedure against the analytical solution given in Krzikalla, F. and Müller, T. (2011). The background has dry modulus K_m=9.15 GPa, shear modulus G=3.16 GPa, porosity ϕ=0.28 and permeability κ=0.37 D, while the corresponding values for the fractures are K_m=0.00722 GPa, G=0.00249 GPa, ϕ=0.64 and κ=18.2 D. In this example, we consider a brine saturated sample, with brine having density ρ_s= 1000 kg/m^3 , viscosity μ= 0.001 $Pa \cdot s$ and bulk modulus K_f=2.25 GPa.

  qP waves show velocity anisotropy and strong attenuation along directions normal to the fracture layering, qSV waves have stronger velocity anisotropy than qP waves, maximum attenuation at about 45 degrees and no loss along the directions parallel and normal to the fracture layering. Velocity of qSV waves has the typical cuspidal triangles (triplications), observed in fractured media. SH waves are lossless and show velocity anisotropy.

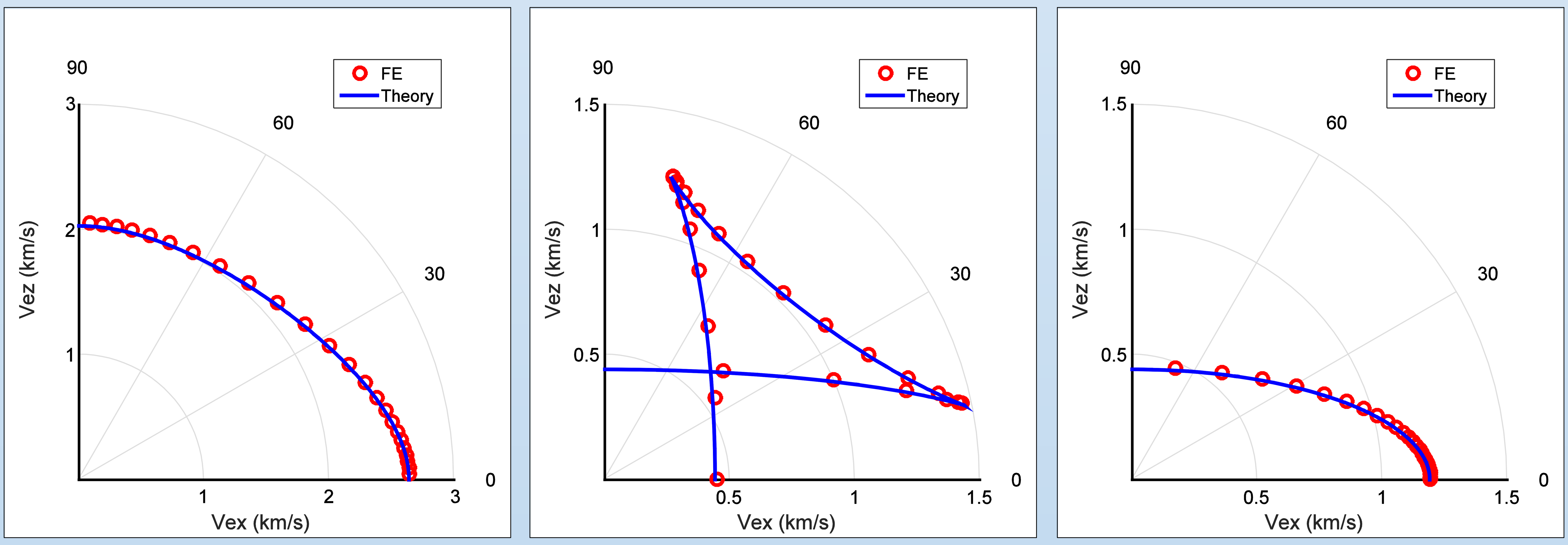

(a) (b) (c)

Polar representation of the energy velocity as function of the propagation angle. Frequency is 60 Hz. The symbols correspond to the FE experiments, while solid lines indicate the analytical values. (a) qP waves. (b) qSV waves. (c) SH waves.

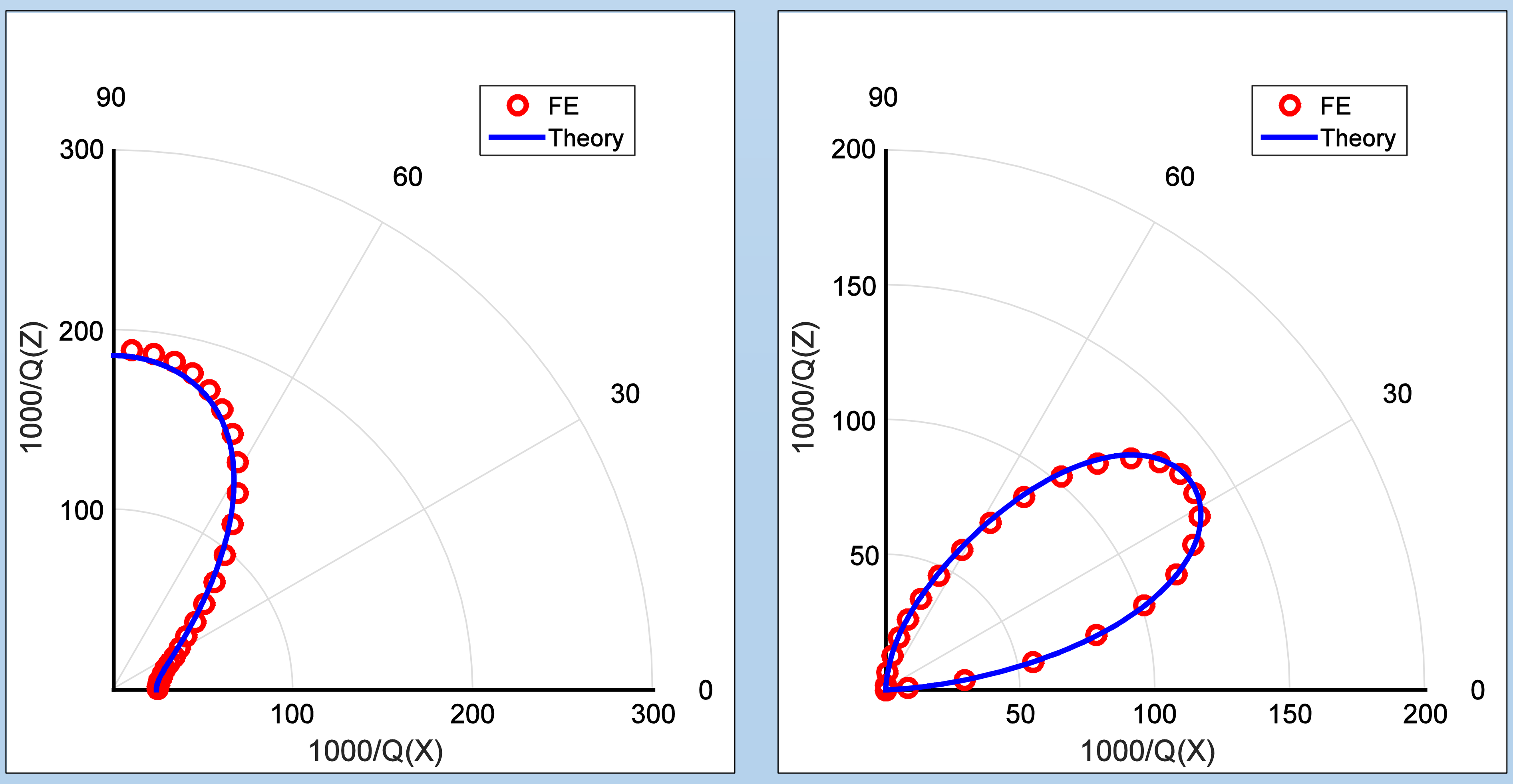

(a) (b)

Polar representation of the dissipation factor [(1000/Q)(sinθ, cosθ)] as function of the propagation angle. Frequency is 60 Hz. The symbols correspond to the FE experiments, while solid lines indicate the analytical values. (a) qP waves. (b) qSV waves.

- The second experiment considers the same sample but for full brine saturation, full gas saturation and 15% and 50% patchy brine-gas saturation. Brine has the same properties of the first experiment, while gas has density 78 kg/m^3, viscosity 0.00015 $Pa \cdot s$ and bulk modulus 0.012 GPa. Frequency is 60 Hz and a 100 × 100 mesh was employed.

Velocity of qP waves decreases as gas saturation increases, while qP anisotropy is enhanced by patchy saturation, and decreases as gas saturation increases. For qSV waves, velocity decreases as gas saturation increases, dissipation factor for qSV waves, shows maximum attenuation at 15% gas saturation, and decreasing anisotropy as gas saturation increases. Patchy saturation breaks the symmetry of the curves (see the cuspidal triangles).

In the fluid pressure distribution, the higher pressure values occur at the fracture locations, while the darker regions values identify the gas patches.

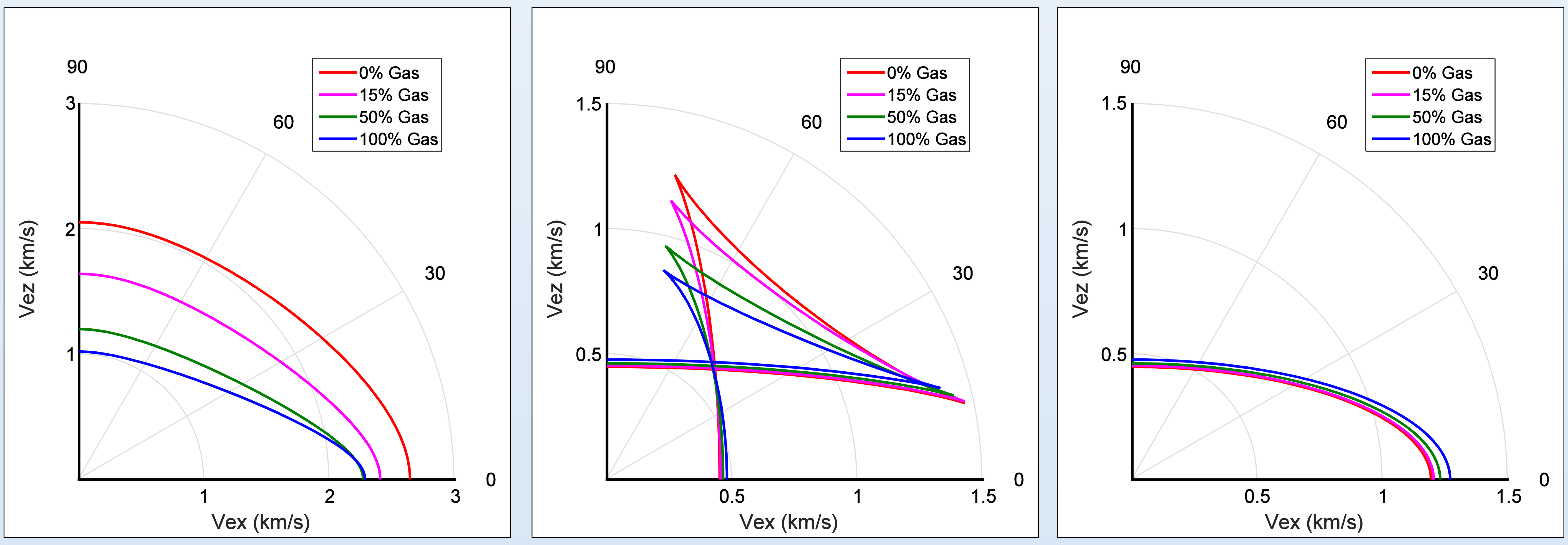

(a) (b) (c)

Polar representation of the energy velocity as function of the propagation angle for full brine, full gas, 15% and 50% patchy gas-brine saturation. Frequency is 60 Hz. (a) qP waves. (b) qSV waves.

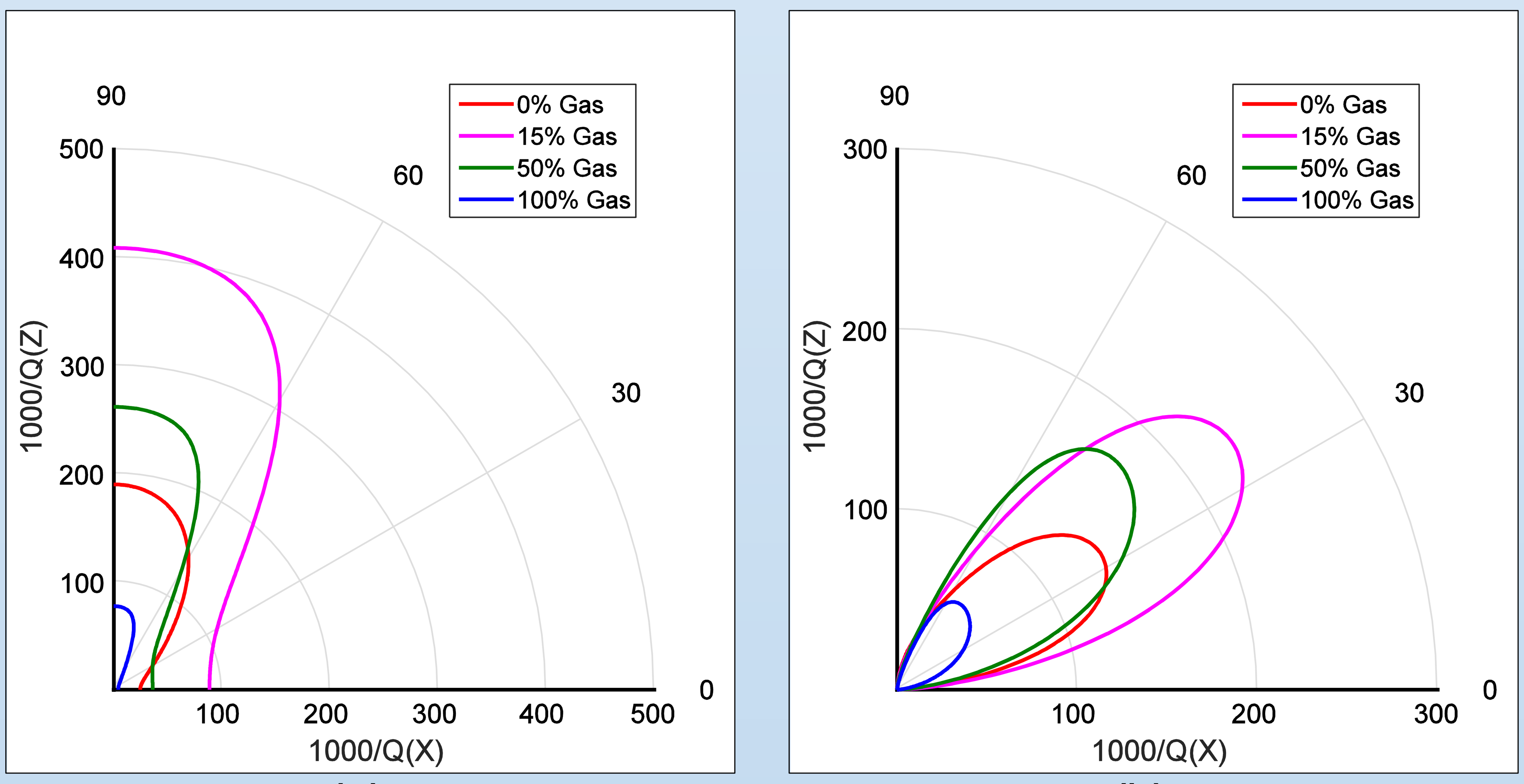

(a) (b)

Polar representation of the dissipation factor [(1000/Q)(sinθ, cosθ)] as function of the propagation angle. Frequency is 60 Hz for full brine, full gas, 15% and 50% patchy gas-brine saturation. (a) qP waves. (b) qSV waves.

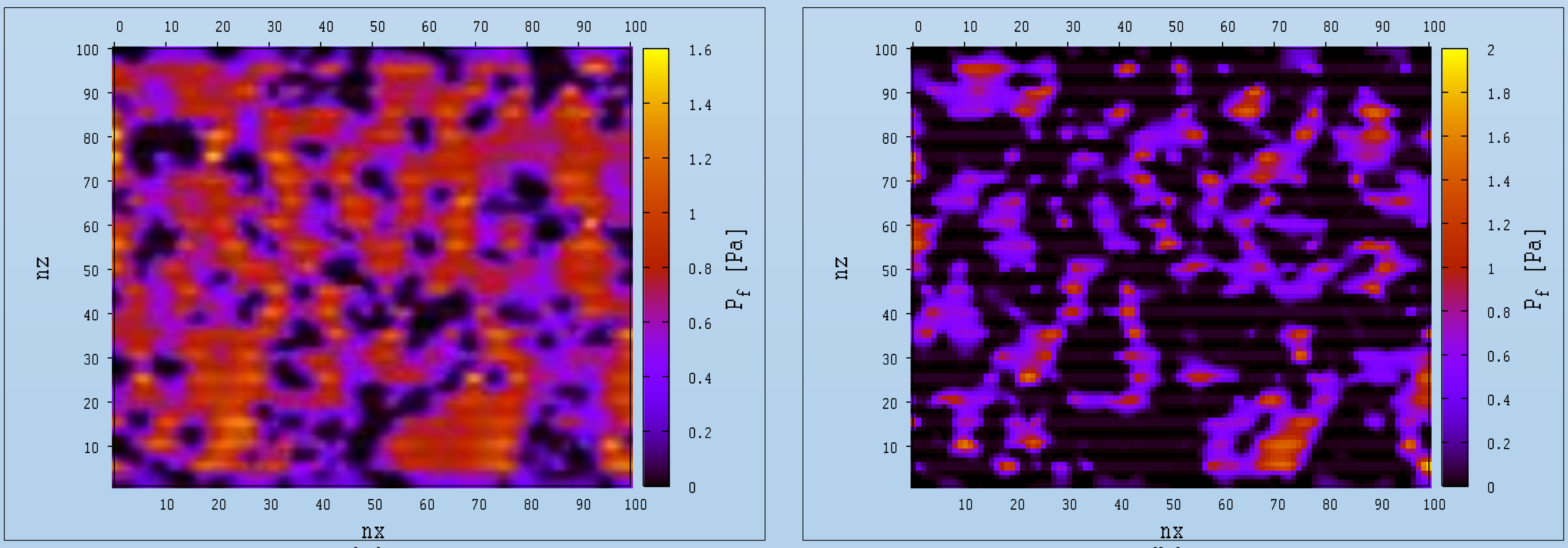

(a) (b)

Fluid pressure for normal compression to the fracture plane at 15% and 50% patchy gas-brine saturation. Frequency is 60 Hz. (a) 15% Gas. (b) 50% Gas.

Conclusions

We presented a procedure to determine the five complex and frequency-dependent stiffnesses of the TIV medium equivalent to a fractured Biot medium, with fractures modeled as internal boundary conditions. The methodology is first validated against a theory that holds for homogeneous layers and fluid flow normal to the fracture layering, and then applied to the case of patchy gas-brine saturation.